Supporting Information

On the origin of the improved hydrogen evolution reaction in Mn and Co doped MoS_2

Pasquale Orgiani, [a] Luca Braglia, [ab] Vincent Polewczyk, [a] Zhiwei Nie, [c] Francesco Lavini, [d] Shyni Punathum Chalil, [a] Sandeep Kumar Chaluvadi, [a] Piu Rajak, [a] Floriana Morabito, [ab] Edvard Dobovičnik, [e] Vittorio Foglietti, [f] Piero Torelli, [a] Elisa Riedo, [d] Regina Ciancio, [ab] Nan Yang, [c] and Carmela Aruta* [f]

[a.] *CNR-IOM, Strada Statale 14, km 163,5 Basovizza, Trieste 34149, Italy.*
[b.] *Area Science Park, Padriciano 99, Trieste 34149, Italy.*
[c.] *School of Physical Science and Technology, ShanghaiTech University, Shanghai 201210, China.*
[d.] *Tandon School of Engineering, New York University, New York, NY 11201, USA.*
[e.] *Department of Engineering and Architecture, University of Trieste, Trieste 34127, Italy.*
[f.] *CNR-SPIN, via del Fosso del Cavaliere 100, Roma 00133, Italy. Email: carmela.aruta@spin.cnr.it.*

1. Raman Spectroscopy

In Figure S1 is reported the Raman spectra of the MoS_2 2ML thick sample grown by pulsed laser deposition (PLD) on (111) Nb-doped $SrTiO_3$ (NbSTO) substrate. As expected, the Raman peaks of MoS_2 (E^1_{2g}~384 cm^{-1} and A_{1g}~405 cm^{-1}) are superimposed on the strong NbSTO substrate background and hardly identified.[1] The relative position of the peaks $\Delta k(A_{1g}- E^1_{2g})$ ~ 21.5 cm^{-1} agrees well with literature values for PLD samples and confirms the 2ML thickness of the sample.[2]

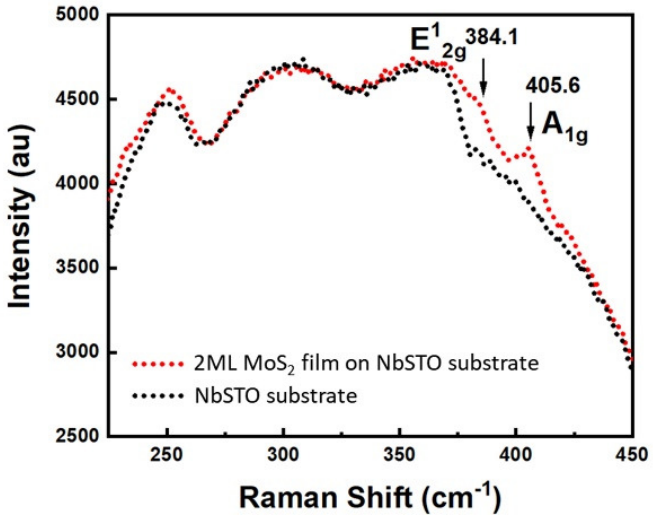

Figure S1. Raman spectra of 2ML MoS_2 film grown on NbSTO substrate compare with the bare NbSTO substrate.

2. High Resolution Transmission Electron Microscopy

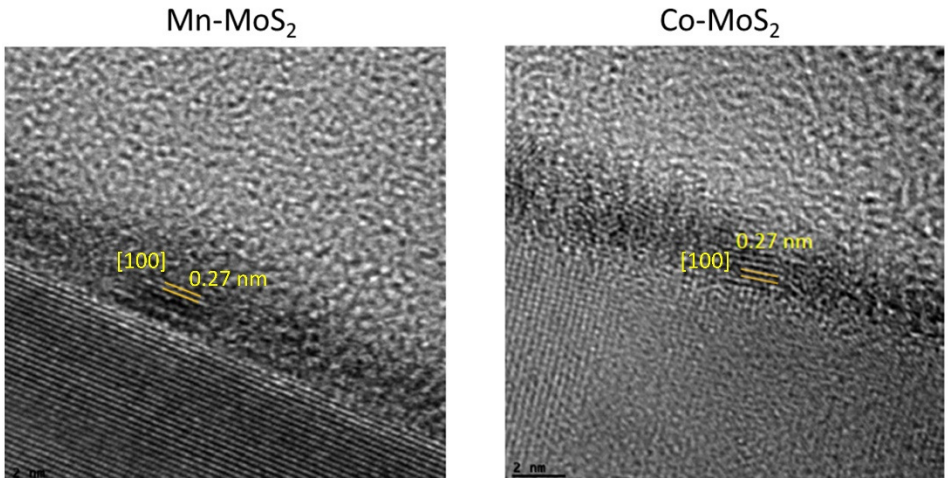

Figure S2. HRTEM image of Mn-doped MoS_2 (Mn-MoS_2) and Co-doped MoS_2 (Co-MoS_2) 2 ML thick.

3. X-ray diffraction measurements

Structural properties of undoped and Mn/Co-doped MoS_2 were carried out by X-ray diffraction (XRD). Since the Mn/Co doping was realizing by a double-target deposition process, to prevent Mn/Co segregation, MoS_2 and metallic Mn/Co targets were alternated after each unit cell of MoS_2. The growth deposition rate was lowered to about 324 laser shots per unit cell thus making the growth of doped MoS_2 very long. As a consequence, relatively thin films (≤20nm) only were investigated.

XRD spectra of a pure MoS_2 film is reported in Figure S3. It shows the presence of multiple diffraction peaks demonstrating the polycrystalline nature of the films.

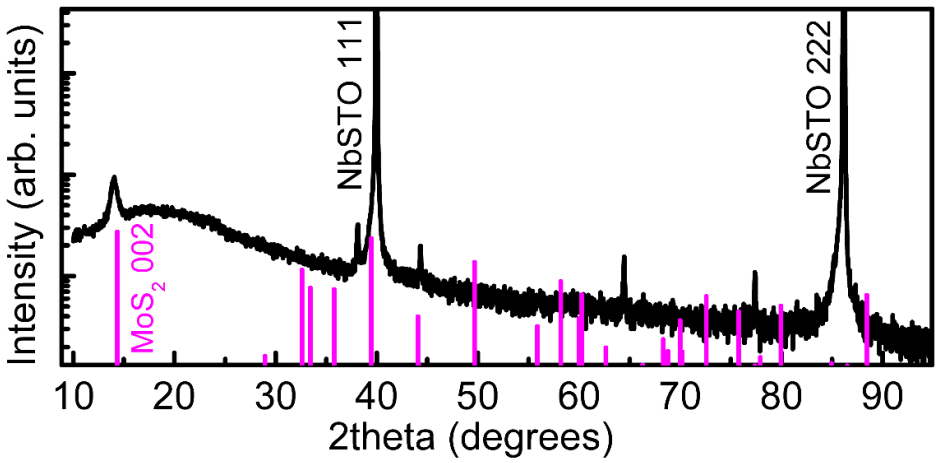

Figure S3. XRD spectra of undoped MoS_2 on NbSTO substrate.

In Figure S4 the XRD measurements across the (002) diffraction peak of undoped and doped MoS_2 films are reported.

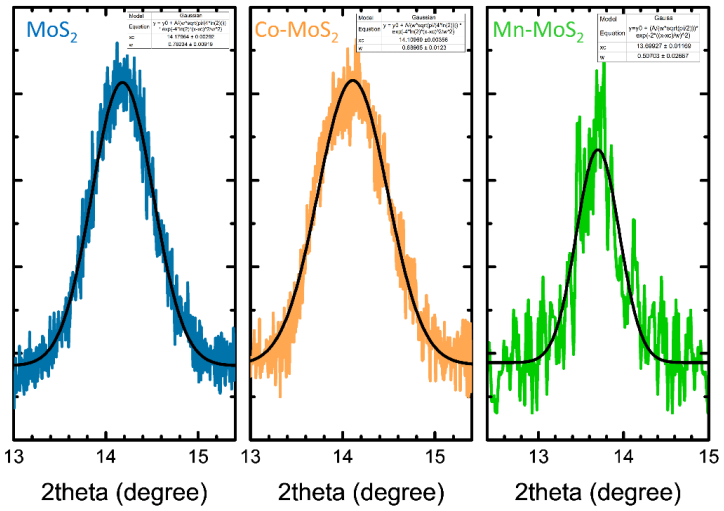

Figure S4. XRD measurements across the (002) reflection: (a) undoped MoS2, (b) Co doped MoS2 and (c) Mn doped MoS2.

In the case of doped samples a shift of the (002) diffraction peak is observed corresponding to an increase in the lattice parameter. According to Shannon's database of ionic radii the Mo^{6+} ionic radii ranges from 0.41 to 0.73Å; however, both Co^{2+} and Mn^{2+} ionic radii are larger than Mo^{6+}, namely Co^{2+} ranges from 0.58 to 0.90 Å while Mn^{2+} from 0.66 to 0.96Å, respectively.[3] Therefore, the enlargement of the lattice parameter of doped films is compatible with the Mo-Mn/Co substitution.

4. Scanning Electron Microscope/Energy-dispersive X-ray spectroscopy

During the optimization of the growth process we used a Scanning Electron Microscope (SEM) equipped with a detector for Energy-dispersive X-ray spectroscopy (EDX) to get the ablation rate per laser shot. Reliable information on the quantitative Mo:S stoichiometric amounts was obtained on thick MoS_2 films grown on Al_2O_3 substrate, for which the overlap between the characteristic EDS peaks are negligible (see Figure S6). The Mo:S chemical ratio was found to be 38:62, which is very close to the expected value of 33:66, thus indicating a correct stoichiometry of the MoS_2 grown films.
However, the ablation rate of both Mn and Co metallic disk was realized by keeping fixed the number of laser shots (i.e. 3000) for all of the targets (i.e. MoS_2, Mn and Co) and evaluating by EDS the overall MoS_2:Mn:Co stoichiometric ratio. As following the EDS spectrum clearly showing all of the expected peaks. In particular, the stochiometric MoS_2:Mn:Co stoichiometric ratio was found 64.9:31.3:3.8, therefore setting the laser-shots needed for a aimed composition for Mn/Co-doped MoS_2 films (Figure S7).

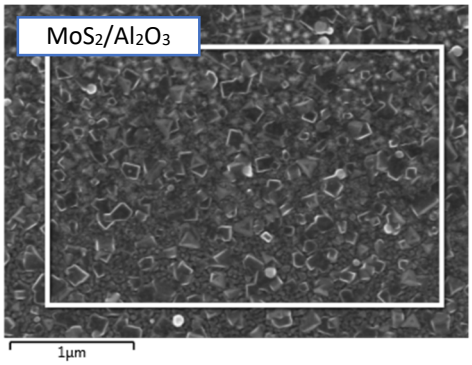

Figure S5. Surface morphology by Scanning Electron Microscope (SEM) of a MoS_2 film grown on Al_2O_3 susbtrate.

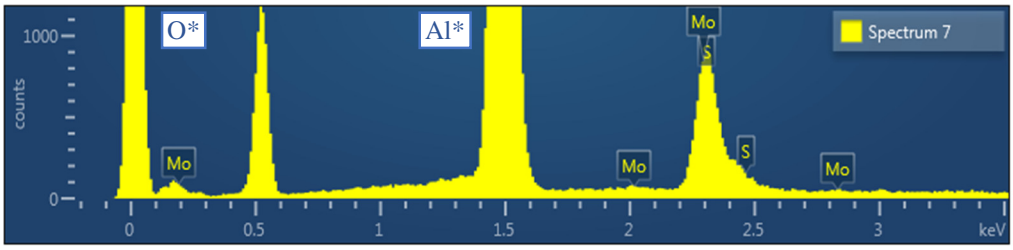

Figure S6. EDX spectra of MoS_2 films grown on Al_2O_3 substrate.

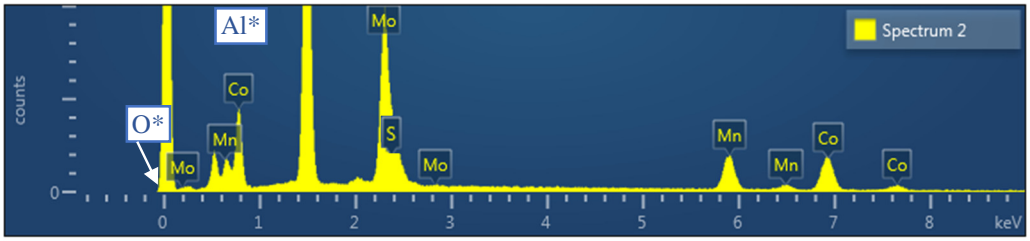

Figure S7. EDX spectra of Mn/Co-doped MoS_2 films grown on Al_2O_3 substrate.

5. Kelvin Probe Force Microscopy

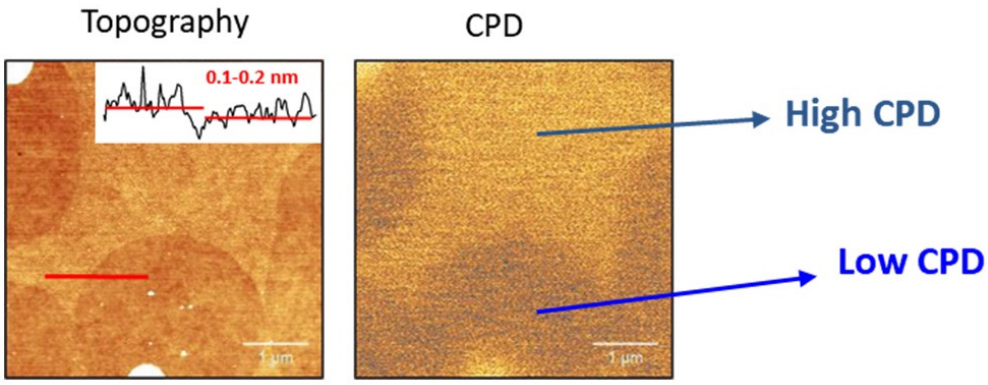

Figure S8. Topography on the left and contact potential difference (CPD) on the right images of 2ML undoped MoS_2 sample.

4. Electrochemical characterizations

The image processing of the picture in Figure S9 give the geometric area reported in Table S1.

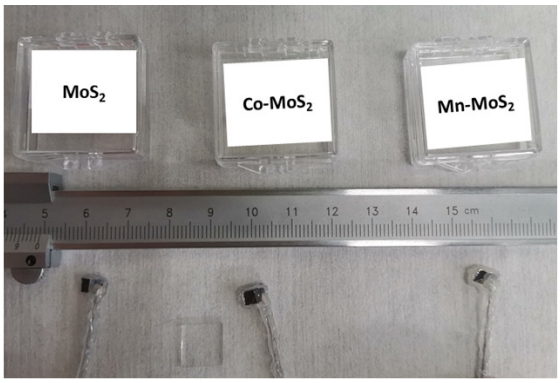

Figure S9. Picture of the electrode fabrication for the electrochemical properties.

The mass activity is the activity per unit mass that can be useful to evaluate and compare the catalytic activity of different samples.[4] It is the current density normalized to the mass of the sample. The volume is obtained by the geometric area product for the 20 nm thickness and we used the MoS_2 density ρ=4.05 g/cm^3. [5] The results are reported in Figure S10 as a function of potential.

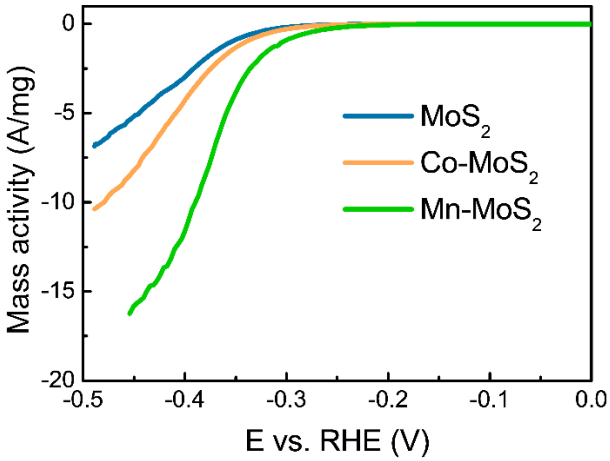

Figure S10. Mass activity as a function of potential.

The whole set of electrochemical impedance spectroscopy (EIS) measurements are shown in Figure S11 on undoped MoS_2, 6% Mn doped MoS_2 (Mn-MoS_2) and 7% Co doped MoS_2 (Co-MoS_2) with a thickness of 20nm. The frequency range is 200 kHz - 200 mHz.

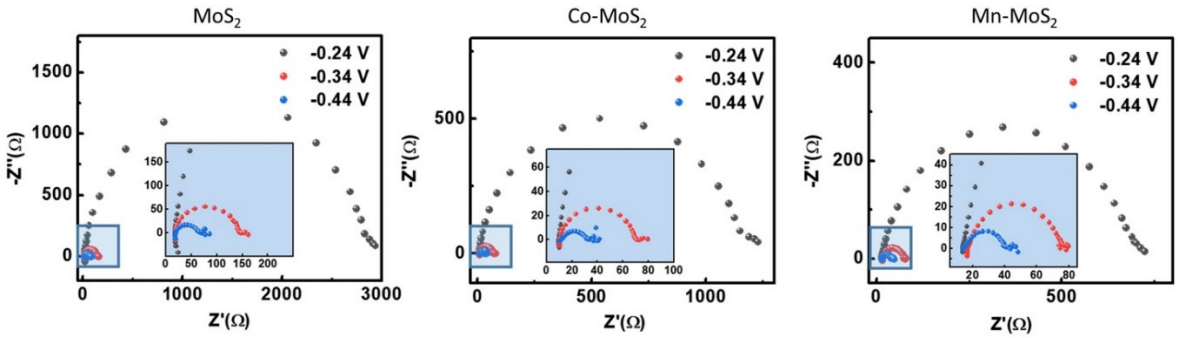

Figure S11. Electrochemical impedance spectroscopy measurements for undoped and doped MoS_2.

Cyclic voltammetry (CV) measurements for the undoped MoS_2 and doped with Co and Mn are reported in Figure S12. The same CV measurements have been repeated for 500 cycles to test the stability of the samples. The linear sweep voltammograms, i.e. the current density as a function of potential, are compared before and after 500 cycles of CV measurements and shown in Figure S12.

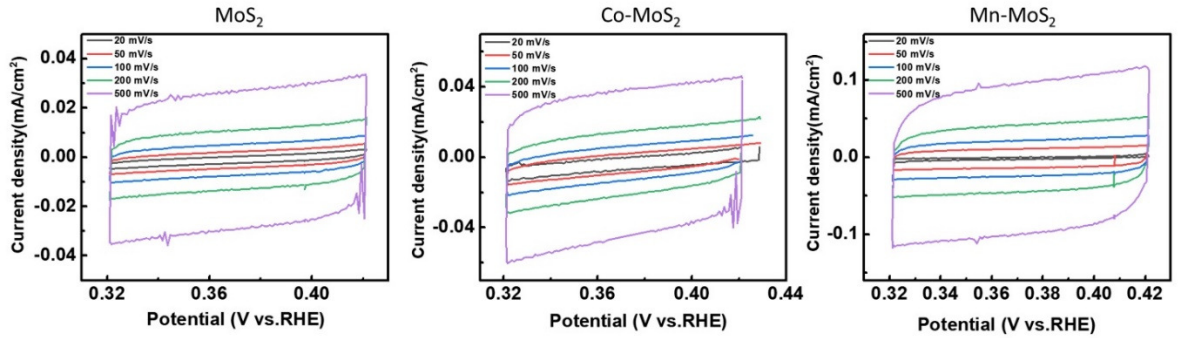

Figure S12. Cyclic voltammetry (CV) measurements for the undoped MoS_2 and doped with Co and Mn.

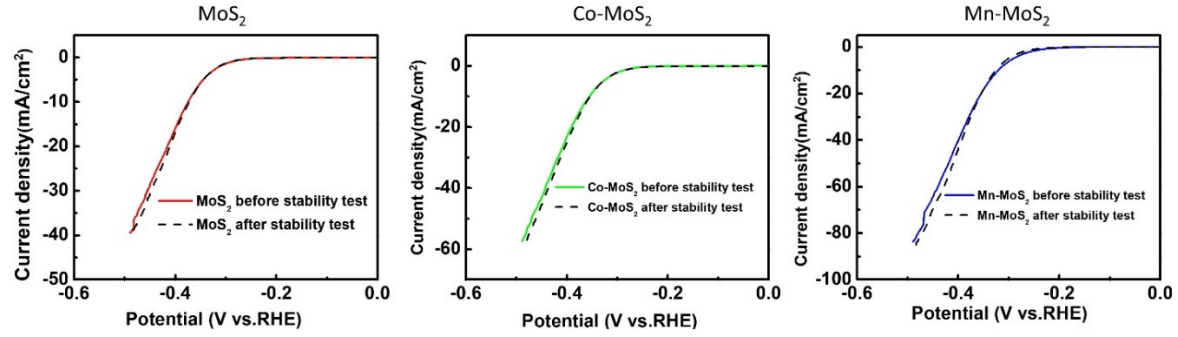

Figure S13. Comparison between the current density as a function of potential before and after the stability test for the undoped MoS_2 and doped with Co and Mn.

sample	MoS_2	Co-MoS_2	Mn-MoS_2
Onset (V)	-0.3	-0.28	-0.23
η10 (V)	-0.36	-0.35	-0.31
Tafel slope (mV/dec)	81	80	79
J_0 (mA/cm^2)	3.27 10^{-4}	4.41 10^{-4}	1.23 10^{-3}
Rs(Ω)	18.4	10.4	17.1
R_{ct}(Ω)	127.3	60.5	57.1
ECSA	0.825	1.32	2.91
A_{geom} (cm^2)	5.6 10^{-2}	8.1 10^{-2} cm^2	5.0 10^{-2} cm^2
$A_{specific}$ (cm^2)	0.05 cm^2	0.10 cm^2	0.14 cm^2

Table S1. Main parameters obtained from the electrochemical measurements: Onset = potential with current density > 1 mA/cm^2; η10 = potential at which current density increases over 10 mA/cm^2; Tafel slope= slope by fitting the plot of overpotential versus log (current density) by Tafel equation; j_0 = exchange current density; R_s = imaginary part equal to zero at high frequency; R_{ct} = charge transfer resistance; ECSA (C_{dl}/C_s)= Electrochemical Surface Area; A_{geom} = geometric area from the picture in Figure S9; $A_{specific}$ ($A_{geom} \times$ ECSA)=specific active surface.

5. X-ray Photoemission Spectroscopy

Mo 3*d* and S2*p* core level spectra were measured for the undoped samples, as well as Mn 2*p* and Co 2*p* were measured for the doped ones. The fitting procedure was performed after the Shirley background subtraction, while keeping fixed as much as possible the fitting parameters. For the Mo 3*d* we used two couples of $3d_{5/2}$ and $3d_{3/2}$ spin-orbit doublets for the Mo^{4+} and a higher binding energy (BE) contribution (higher valence state, Mo^{HV}), as shown in the main text. A small contribution from the Mo^{6+} at even higher BE is hardly detectable, also thanks to the in-situ transferring of the samples to the XPS analysis chamber, which prevents from surface oxidation.
In the fitting procedure the spin orbit splitting was fixed at 3.14 eV for all the doublets, the degeneracy ratio was 2:3 for the spin-orbit area ratio and the full width at half maximum (FWHM) was a free parameter but fixed at the same value for the two peaks of each doublet. For the S 2*p* we also used the minimum number of components to fit the doublet of the $2p_{3/2}$ and $2p_{1/2}$ spin-orbit splitting. The splitting was fixed at 1.2 eV for all the components, the degeneracy ratio was 1:2 for the spin-orbit area ratio and the FWHM was a free parameter but the same for both peaks of each doublet.
The relative area of Mo^{HV} with respect to Mo^{4+} results about 21% for MoS_2, 14% for Mn-MoS_2 and 15% for Co-MnS_2. It determines the observed shift of the Mo 3*d* spectra to lower BE reported in the main manuscript.
In the doped samples we performed the fit of the Mn 2*p* and Co 2*p* core level spectra. The fit shown in the main manuscript is performed considering non-local and local screening components (labelled as A and B, respectively) in the main peaks $2p_{3/2}$ and $2p_{1/2}$.[6-8] We also included the shake-up satellites resulting from the ligand-to-metal

charge transfer during the photoemission process which can be interpreted, at the simplest level of approximation, by a molecular orbital description.[9-11] We fixed the degeneracy ratio of 2:1 for the two spin–orbit coupling components $2p_{3/2}$ and $2p_{1/2}$ for both Mn 2*p* and Co 2*p* core levels and the splitting was fixed at 11.44 eV for Mn 2*p* and 15 eV for Co 2*p*, respectively. The contribution of the shake-up satellites at about 5.8 eV above the main peak for the Mn 2*p* and Co 2*p* spectra, respectively, was also present. These satellites can be associated to the presence of Mn^{2+} and Co^{2+} valence state contribution.

The stoichiometry was obtained for all the investigated samples from the fitting of the survey scans measured at excitation energy of 1100 eV using interpolated atomic cross sections. We obtain that S decreases from 63.3% in the undoped MoS_2 to about 62.8% for 5% Mn-MoS_2, down to about 54.7% for 23% Mn-MoS_2. The results are shown in Figure S7.

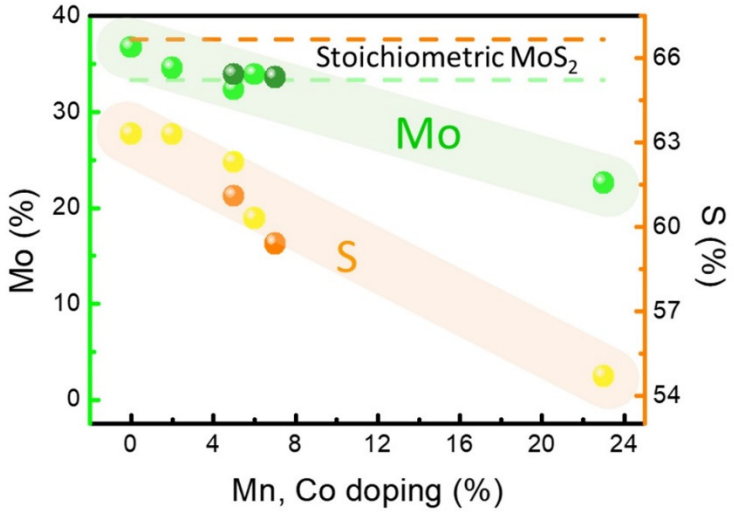

Figure S14. Compositional analysis of undoped MoS_2 and doped with different Mn and Co concentrations: light green symbols correspond to Mo concentration in Mn-MoS_2, dark green symbols correspond to Mo concentration in Co-MoS_2, yellow symbols correspond to S concentration in Mn-MoS_2, orange symbols correspond to S concentration in Co-MoS_2. The dashed lines correspond to the stoichiometric values for MoS_2 useful for comparison, green for Mo and orange for S.

6. Valence band fit

The qualitative fit of the VB region of undoped MoS_2 is reported in Figure S8 for the off- and on-resonance measurements. According to the theoretical calculations reported in literature, the contribution of Mo 4*d* is spread over all the VB spectra.[12] However, the S 2*p* contribution approximately occurs mainly above 5 eV. Therefore, we can consider the A and B features associated to the Mo $4d_{z2}$ and Mo $4d_{xy}$ bands respectively, while the feature C, and with less extent feature D, associated to the Mo-S hybridized bands. In the case of on-resonance VB spectra we added the E band associated to the in-gap states. Band D contains also contribution from the VB of the NbSTO substrate.

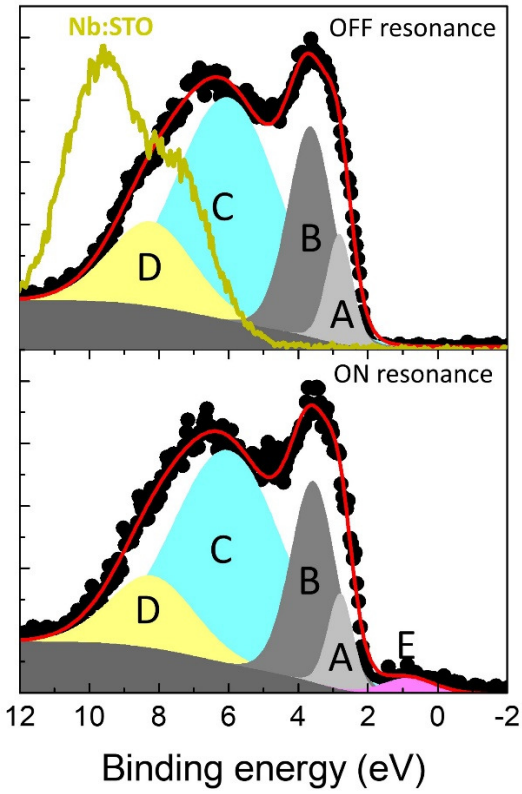

Figure S15. VB fit of undoped MoS_2 20 nm thick film off resonance at 380 eV (top panel) and on resonance 398 eV (bottom panel).

Similarly to the case of RESPES for undoped MoS_2 of Figure S8, the fit of the off-resonance VB measurements of 2ML thick films (Figure S9) is performed with 4 components in the undoped MoS_2 and by adding one more component in the case of Co and Mn doped samples. The contributions between 2 and 4 eV from the Fermi level are the Mo 4*d* bands, while the S 3*p* orbitals occurs above 5 eV.

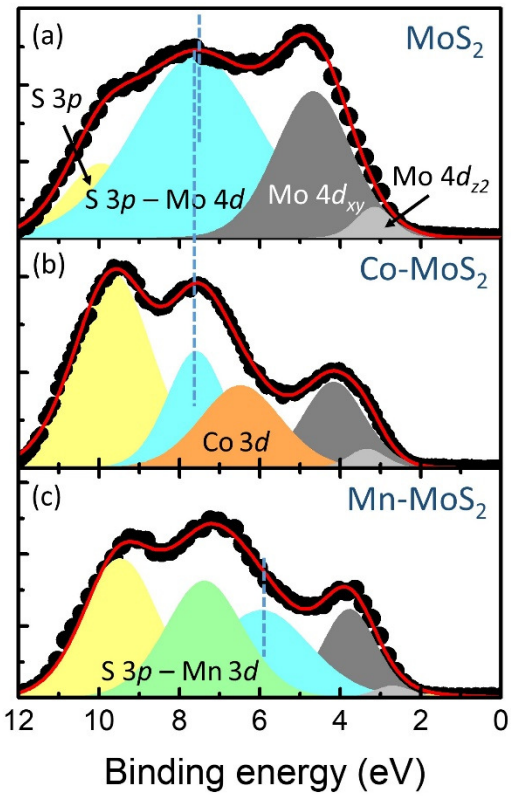

Figure S16. VB measurements off-resonance of 2ML thick MoS_2 samples, undoped in (a), Co-doped in (b) and Mn-doped in (c). Excitation energy 1100 eV.

References

1 W.C. Wong, S.M. Ng, H.F. Wong, W.F. Cheng, C.L. Mak and C.W. Leung, *Solid-State Electron.* 2017, **138**, 62.

2 Y.-T. Ho, C.-H. Ma, T.-T. Luong, L.-L. Wei, T.-C. Yen, W.-T. Hsu, W.-H. Chang, Y.-C. Chu, Y.-Y. Tu, K. Prasad Pande, and E. Y. Chang Ho, *Phys. Status Solidi RRL* 2015, **9**, 187.

3 http://abulafia.mt.ic.ac.uk/shannon/ptable.php

4 J. Kibsgaard and I. Chorkendorff, *Nat. Energy* 2019, **4**, 430.

5 Materials Data on MoS_2 by Materials Project. United States: N. p., 2020. Web. doi:10.17188/1202268.

6 Z. Cai, M. Kubicek, J. Fleig and B. Yildiz, *Chem. Mater.* 2012, **24**, 1116.

7 L. Dahéron, R. Dedryvère, H. Martinez, M. Ménétrier, C. Denage, C. Delmas and D. Gonbeau, *Chem. Mater.* 2008, **20**, 583.

8 M. A. van Veenendaal and G. A. Sawatzky, *Phys. Rev. Lett.* 1993, **70**, 2459.

9 S. Hüfner, Photoelectron Spectroscopy: Principles and Applications, Springer Science & Business Media, 2013.

10 C. R. Brundle and A. D. Baker, Electron Spectroscopy: Theory, Techniques, and Application, Academic Press, New York, 1978.

11 S. Hüfner, *Adv. Phys.* 1994, **43**, 183.

12 L. A. H. Jones, Z. Xing, J. E. N. Swallow, H. Shiel, T. J. Featherstone, M. J. Smiles, N. Fleck, P. K. Thakur, T.-L. Lee, L. J. Hardwick, D. O. Scanlon, A. Regoutz, T. D. Veal, and V. R. Dhanak, *J. Phys. Chem. C* 2022, **126**, 21022.